NRIAG JOURNAL OF ASTRONOMY AND GEOPHYSICS
2021, VOL. 10, NO. 1, 270–278
https://doi.org/10.1080/20909977.2021.1913364

ARTICLE

OPEN ACCESS Check for updates

Gravity interpretation for delineating subsurface structures and depth of basement at El Moghra area, North Western Desert, Egypt

Sultan A.S. A. S. Araffa[a], Maha Abdelazeem[a], Hassan S. S. Sabet[b] and Ahmed M. M. Al Dabour[c]

[a]National Research Institute of Astronomy and Geophysics NRIAG, Helwan, Egypt; [b]Geology Dept. Faculty of Science, Al-Azhar University, Cairo, Egypt; [c]The General Company for Researches and Groundwater &green Valley for Logging, Egypt

ABSTRACT

El Moghra area represents a vital part of the national reclamation area at the northern part of Western Desert, Egypt. Delineating subsurface structures (faults & basins) and depth to the basement is the base of planning the area. Basins can be water aquifers or oil traps. Gravity data has been used to tackle such aims. The gravity (Bouguer) anomaly map is separated into regional components (deep sources), and residual component (shallower sources). The residual gravity map was used to delineate subsurface structural features dissecting the investigated area. Also, Euler deconvolution and Tilt Derivative methods have been used for delineating the structural elements. The gravity interpretation indicates that the most main tectonic have E–W, ENE–WSW, and N–S trends for the major structures, while the minor structures are aligned in NNE–SSW, NE–SW, NNW–SSE, and NW–SE. The results of depth estimation using 2D and 3D modelling show that the eastern and southwestern parts of the area under study exhibit a deep basement structure, reaches more than 7000 m (basin). However, the central and northwestern parts of the investigated area show shallower depth of basement rocks (4100 m).

ARTICLE HISTORY
Received 21 February 2021
Revised 29 March 2021
Accepted 31 March 2021

KEYWORDS
Depth to basement; North-Western Desert; Moghra area; basins; faults; Euler deconvolution; 2d & 3d modelling

1. Introduction

The area under study is important for different oil exploration companies; where it is located in the northern of the Qattara Depression. El Moghra Oasis and its vicinities locate in the north Western Desert; about 40 km south of El Alamein (Figure 1(a)). It extends between latitudes 30°00'–30°25' N and longitudes 28°20'–29°20' E. The gravity data can be used for delineating the subsurface structures and defining the depth of basement rocks to locate the basins which can be referred to as the best locations for oil accumulation (Sultan et al. 2009; Araffa et al. 2014, 2015; Abdelazeem et al. 2020, 2021). The target of the current study aims to determine the basins which can be occupied by oil potentiality or water and faults controlling the subsurface sequence (Abdelazeem et al. 2020).

2. Geology of the study area

Moghra Oasis is covered by different sedimentary rock units ranging in age from Lower Miocene to Quaternary (Figure 1(b)). The Lower Miocene rock units are represented here by Moghra Formation are formed of marine sediments (Said 1962; Pickford et al. 2009). The Middle Miocene sedimentary rocks include the Marmarica Formation, which is composed of fossiliferous carbonates. The Pliocene rock units formed of smoky limestone intercalated with marl interbeds. The northern part of the study area is occupied by Pliocene rock units which are composed of white limestone with shale intercalation and evaporite layers (Omara and Sanad 1975). The Quaternary rocks are found here as sand dunes, sand sheets and sabkha. A sand sheet overlays most areas in Moghra Oasis; Sand dunes occupied the southern part of the area and takes the direction of NW–SE. They are composed of fine to medium sand. In general, the stratigraphic succession of the North-Western Desert is formed of sedimentary rocks belonging to Cenozoic (Miocene, Oligocene & Eocene), Mesozoic (Upper and Lower Cretaceous and Jurassic), and Palaeozoic ages (Figure 1(c)).

3. Gravity data analysis and interpretation

3.1. Gravity data acquisition

The gravity data presented here have been collected by General Petroleum Company (GPC, 1984), which has been digitised for the investigated area forming a Bouguer anomaly map (BAM). The gravity data is usually used to detect subsurface structures utilising disturbance produced at the surface in the earth's gravitational field. The Bouguer gravity anomaly map looks like the topographic contour map. It has circular, elongated and irregular areas of high and low

Corresponding author Sultan A.S. Araffa sultan_awad@yahoo.com National Research Institute of Astronomy and Geophysics NRIAG, Helwan Cairo, Egypt

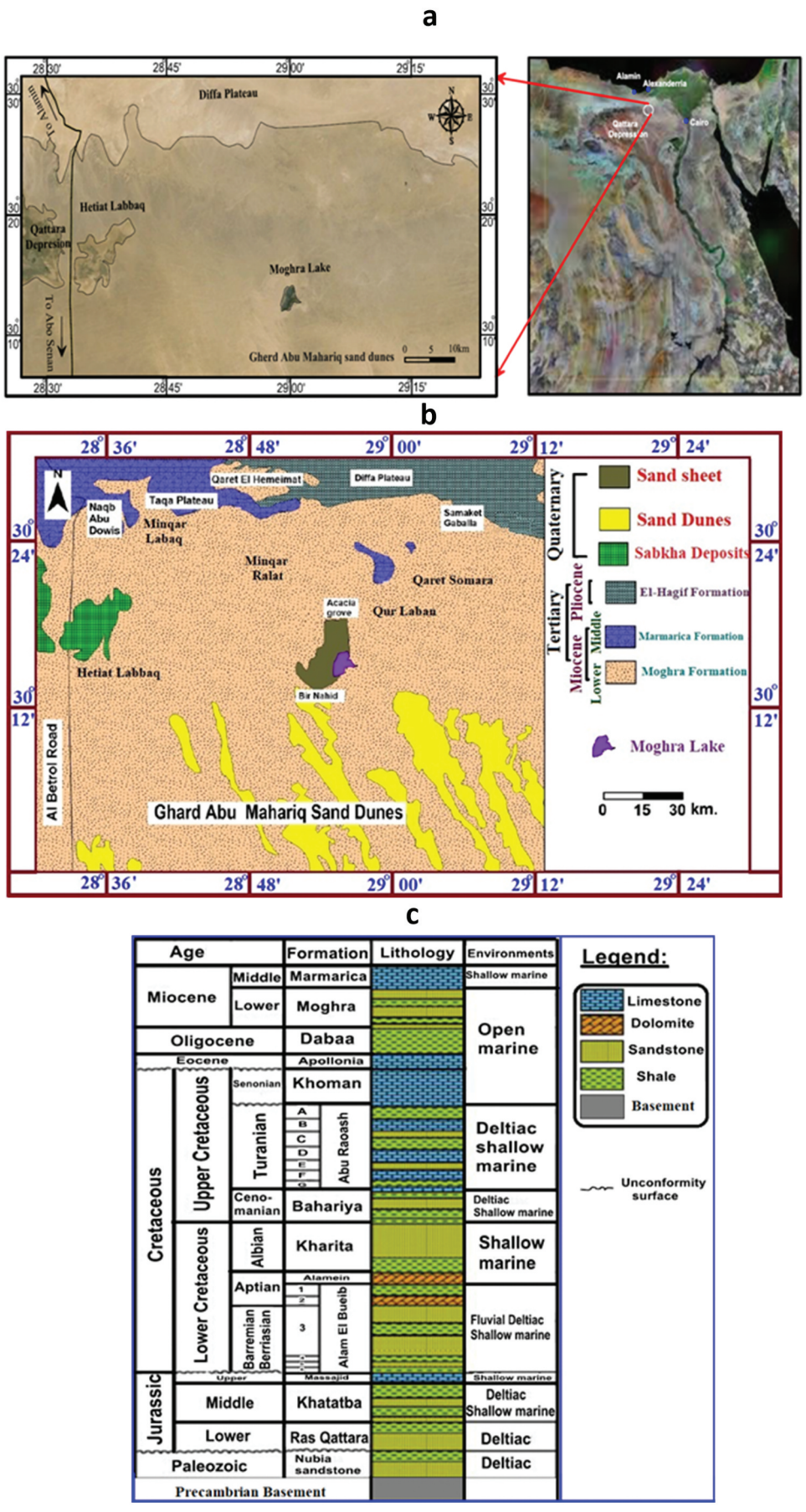

Figure 1. A: Index map, b: Geological map of Moghra Oasis and its vicinities, modified after (CONOCO 1987), c: A generalised stratigraphic section in North Western Desert, Egypt (after Shalaby et al. 2016).

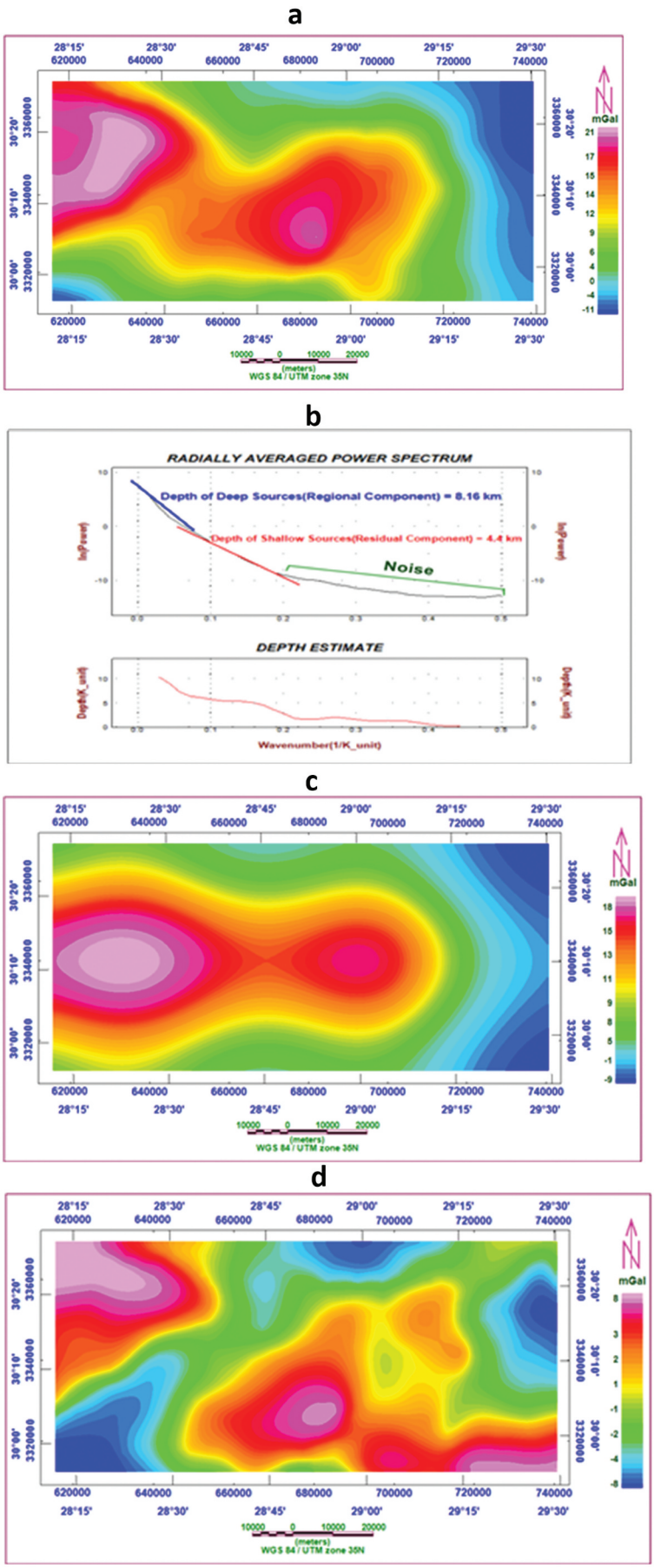

Figure 2. A: Bouguer anomaly map, b: Power spectrum curve, c: low pass (regional) gravity anomy map, d: high pass (residual) gravity anomaly map.

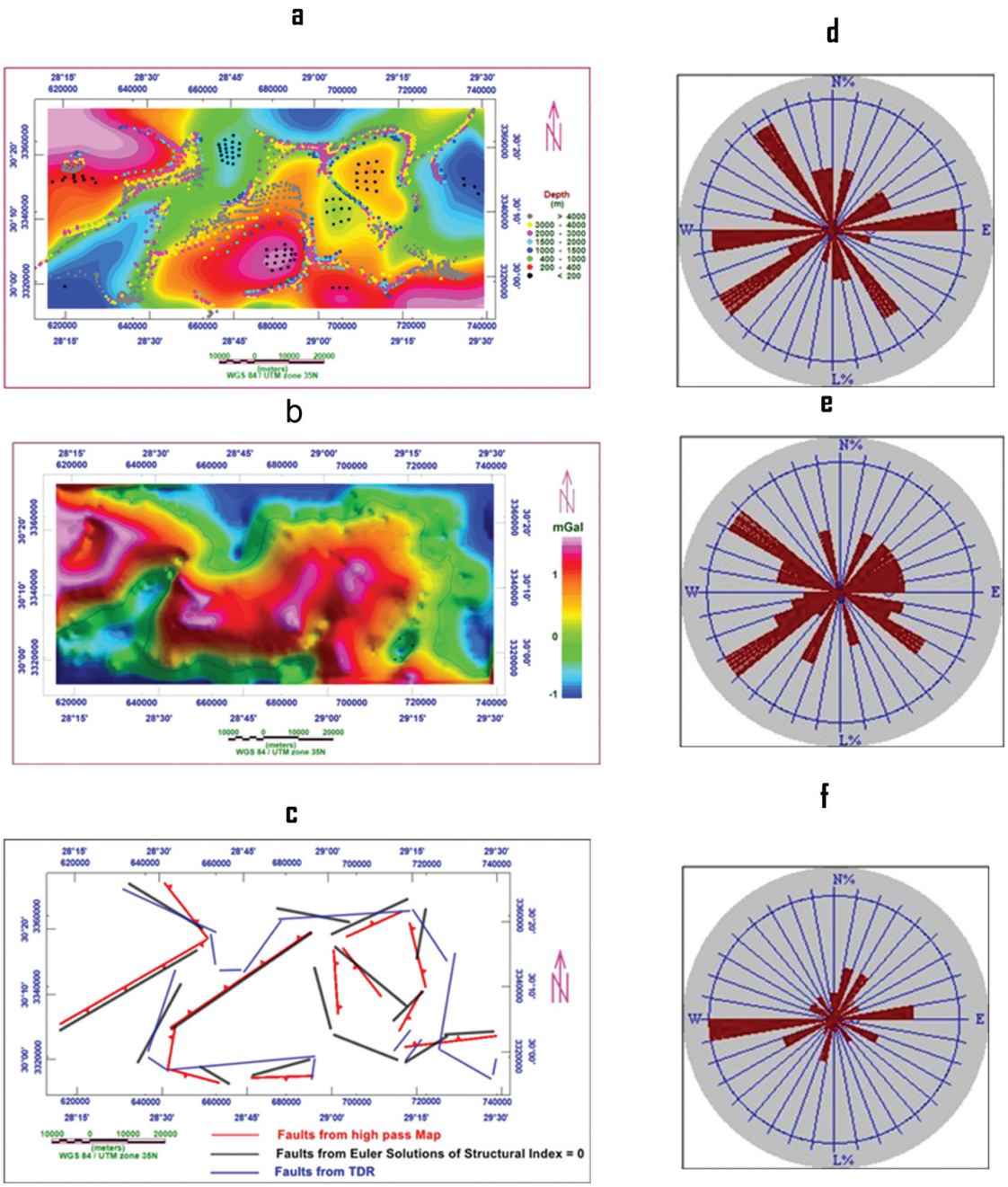

Figure 3. A: residual gravity anomaly map and euler solutions of structural index = 0, b: TDR applied on Bouguer gravity anomaly map of the study area, c: main structural lineaments as deduced from high pass, Euler solutions of structural index = 0 and Tilt Derivative, d: Rose diagrams showing the main structural lineaments as deduced from the high pass map of the studied area, e: rose diagrams showing the main structural lineaments as deduced from the Euler solutions of structural index = 0 map of the studied area, f: Rose diagrams showing the main structural lineaments as deduced from the Tilt derivative map.

Table 1. Main structural trends (Essa 2015).

Principal trend	Mean direction	From	To
N–S	0	N11.25° W	N11.25° E
NNE–SSW	N22.5° E	N11.25° E	N33.75° E
NE–SW	N45° E	N33.75° E	N56.25° E
ENE–WSW	N67.5° E	N56.25° E	N78.75° E
E–W	N90° E or W	N78.75° E	N78.75° W
NNW–SSE	N22.5° W	N11.25° W	N33.75°
NW–SE	N45° W	N33.75° W	N56.25° W
WNW–ESE	N67.5° W	N56.25° W	N78.75° W

gravity values. It may also have linear belts of steep gradient, which are not necessarily associated with any topographic features. The inspection of the BAM in the area (Figure 2(a)) reveals that there is a high gravity value of 21 mGal at central towards Northwestern part of the studied area and a low gravity value of −11 mGal at Northeastern, eastern and southwestern parts of the investigated area.

3.2. Filtering techniques

Different techniques can be used to filtrate the regional component from the residual component. Here, the high and low-pass filters are used for separation. Moreover, many other filters have been applied to

Table 2.: Statistical analysis of high pass map.

Trend	Numbers(N)	Length(L) (Km)	Numbers percentage (N %)	Length percentage (L %)
N–S	2	1.83	16.67	10.89
NNE–SSW	1	0.78	8.33	4.64
NE–SW	0	0	0	0
ENE–WSW	2	4.08	16.67	24.29
E–W	3	3.61	25	21.49
NNW–SSE	0	0	0	0
NW–SE	2	2.33	16.67	13.87
WNW–ESE	1	1.17	8.33	6.96
Total	11	13.8	91	82

Table 3.: Statistical analysis of Euler map.

Trend	Numbers (N)	Length(L) (Km)	Numbers percentage (N %)	Length percentage (L %)
N–S	1	0.85	6.67	4.22
NNE–SSW	1	1.62	6.67	8.04
NE–SW	2	3.43	13.33	17.03
ENE–WSW	4	6.2	26.67	30.78
E–W	3	3.22	20	15.99
NNW–SSE	2	2.04	13.33	10.13
NW–SE	1	1.64	6.67	8.14
WNW–ESE	1	1.14	6.67	5.66
Total	15	20.14	100	100

Table 4. Statistical analysis of the Tilt derivative map.

Trend	Numbers (N)	Length(L) (Km)	Numbers percentage (N %)	Length percentage (L %)
N–S	3	2.68	18.75	14.87
NNE–SSW	2	1.84	12.5	10.21
NE–SW	3	1.28	18.75	7.1
ENE–WSW	1	2.32	6.25	12.87
E–W	3	5.37	18.75	29.8
NNW–SSE	3	3.42	18.75	18.98
NW–SE	1	1.11	6.25	6.16
WNW–ESE	0	0	0	0
Total	16	18.02	100	99

the Bouguer map to investigate the faults controlling the basement structure.

3.2.1. The high– and low-pass filters

The BAM, which is gridded before and contoured using Oasis montaj package (Oasis Montaj Programs 2008) is filtered into regional and residual maps (Figure 2(c,d)) using wavenumber 0.0000143 (1/k_unit) from the power spectrum curve (Figure 2(b)).

The residual (high pass) gravity anomaly map (Figure 2(d)) represents gravity response from shallow sources and after removing the regional effect. The residual map in the study area has a high gravity value of 8 mGal at NW, S, SE, and central parts of the study area and a low gravity value of −8 mGal at N, NE, and SW parts of the study area.

3.2.2. Euler solutions

Euler deconvolution technique was applied on Bouguer map to delineate the depth of gravity sources and trends of structural elements using the structural index (SI) of 0 (Oasis Montaj Programs 2008), the results are plotted on the residual gravity anomaly map as in (Figure 3(a)). Also, the trend of faults at SI = 0 is nearly similar to fault trends which detect from residual gravity anomaly map dissecting by faults (Figure 3(a)).

3.2.3. Tilt Derivative method (TDR)

The TDR technique calculates the TDR of a grid. The TDR filter was applied to the BGAM. The tilt angle derivative filter mostly places the anomaly directly over its source. The zero-contour in the TDR map is located above the fault/contact. Also, the depth is half the distance between the 45o and −45o contours. The TDR of BGAM (Figure 3(b)) shows a lineament of trends NE–SW, N–S, NW–SE, and E–W.

3.2.4. Trend analysis technique

Trend analysis is highly recommended for statistical understanding of geological and geophysical data (Fergany et al. 2014; Abdel; Azeem et al. 2014; Abd El-Azeem et al. 2013). Trends deduced from applying different filters (high pass, Euler & TDR) are represented on rose diagrams (Figure 3(d-f)). These results (direction, numbers, and length) were summarised in (Tables 2, 3, and 4), which generally shows eight main trends. These trends have the following seven principal common directions: N–S, NNE, NE, ENE, E–W, NW, and NNW. A significant discussion of these interpreted trends is given hereafter. The local terminology of the principal structural trends assigned by numerous geoscientists in Egypt in mutual relationship with a universal geometrical classification of the eight main trend directions (N–S, E–W, NNE–SSW, NE–SW, ENE–WSW, NNW–SSE, NW–SE, and WNW–ESE) were gathered and presented in (Table 1) (Essa 2015).

The dominant tectonic trends resulted are generally aligned in E–W, ENE–WSW, and N–S for the major structures, while the minor structures are aligned in NNE–SSW, NE–SW, NNW–SSE, and NW–SE.

3.2.5. Upward continuation maps

Upward continuation minimises the effects of shallow sources and noise in the grid. It is used in interpretation to compare measurements made at different flight elevations (Jacobsen 1987; Telford and Sheriff 1990; Blakely 1995). A series of upward continuation filters were applied to the Bouguer anomaly data. Five maps (Figure 4) at different levels (500 m, 1000 m, 3000, 5000, and 8000 m). Comparing the figures, the upward at a distance of 8000 m upward continuation shows more smoothing feature than the others.

3.2.6. Downward continuation maps

Downward continuation enhances the response from shallow sources (enhancing the short wave responses). A series of downward sessions applied to the data to

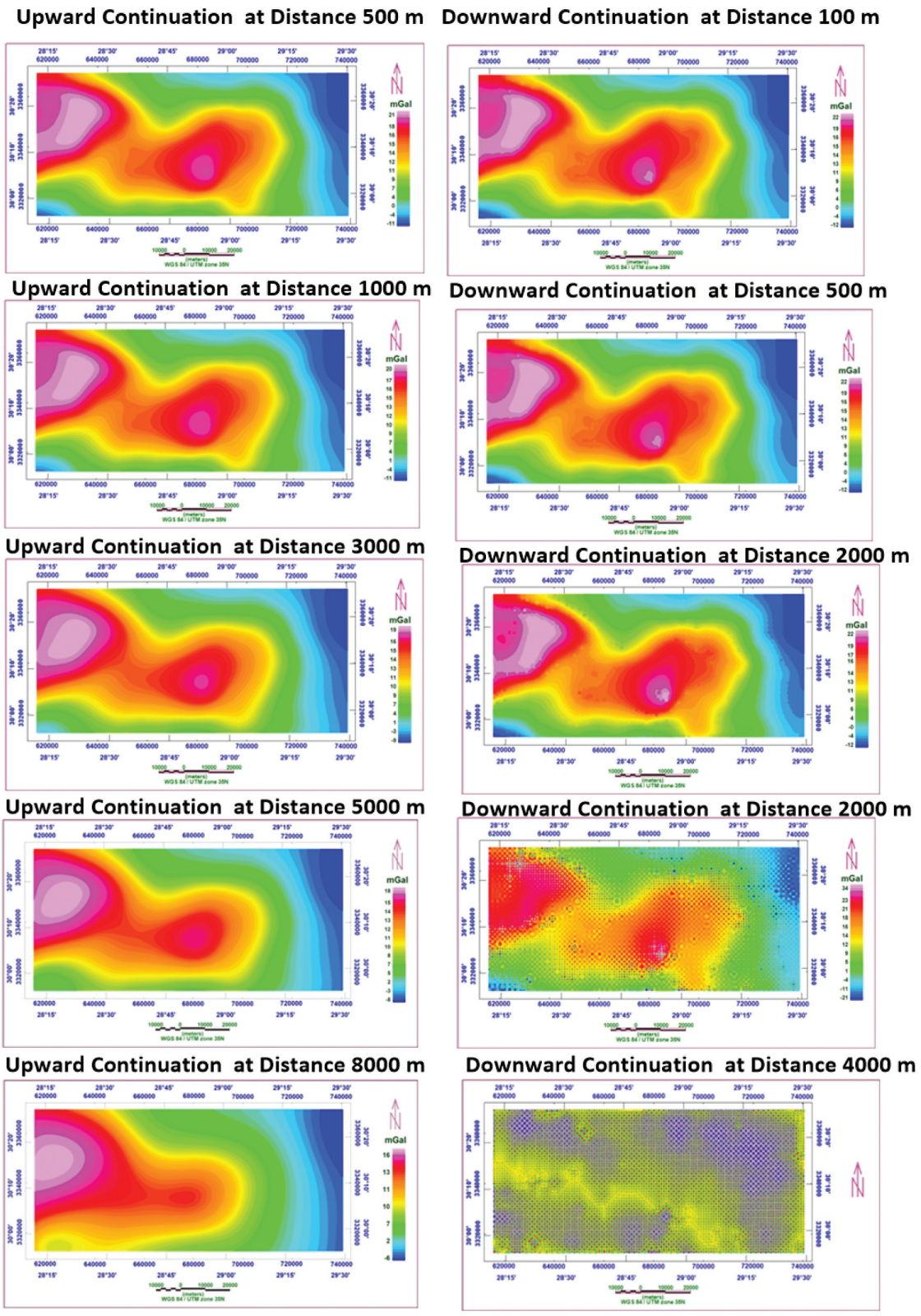

Figure 4. Upward continuation and downward continuation maps.

construct five downward continuation maps started with depth 100 m to 4000 m.

By looking at the downward continuation maps with spaces falling from 100 m to 2000 m (Figure 4), we find that the effect of low and high anomalies started to be distorted. By increasing the depth gradually up to 4000 m (Downward continued map) we will observe a complete deformation of the structure parameters.

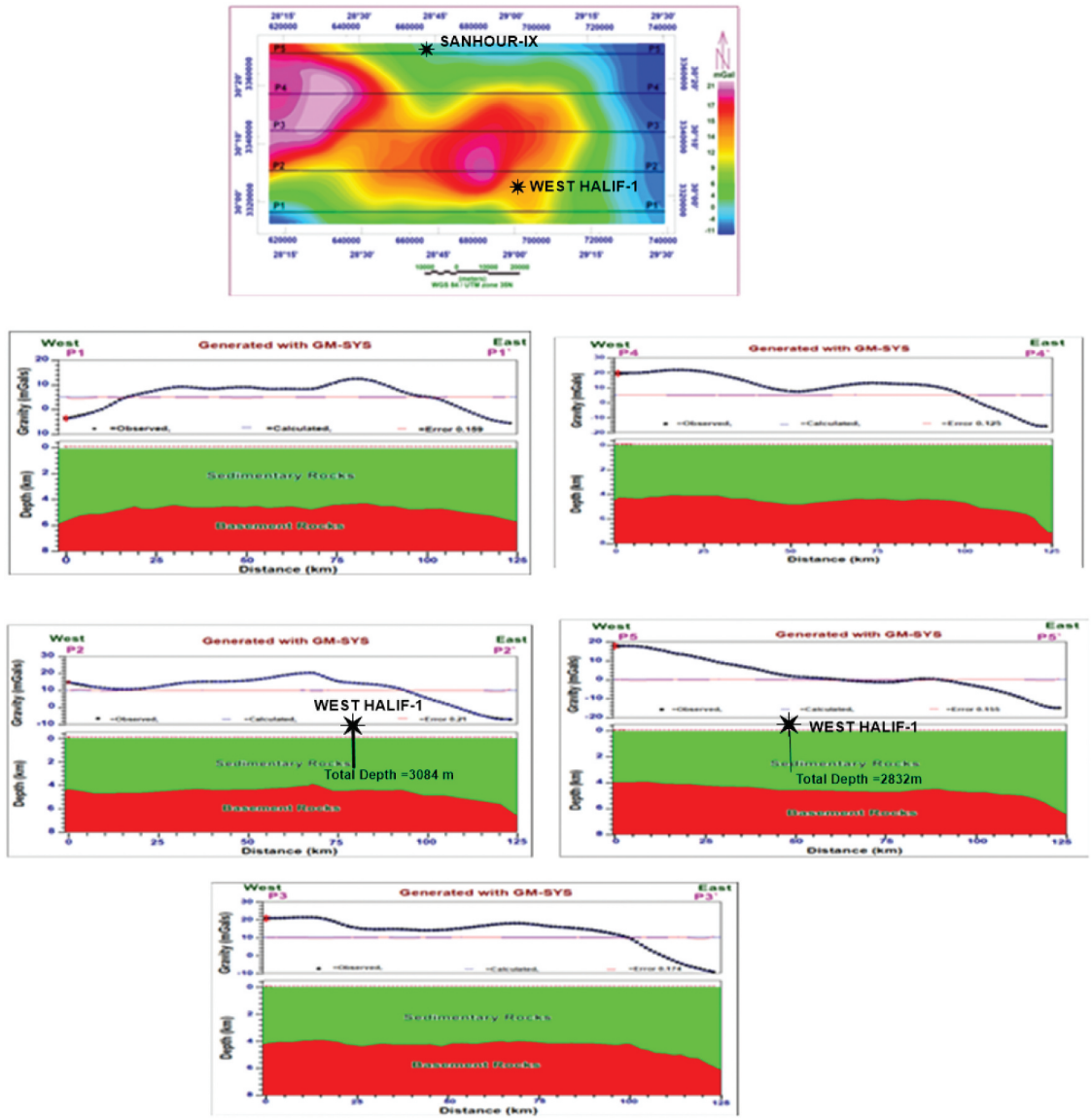

Figure 5. 2D Gravity modelling along profiles P1, P2, P3, P4 and P5.

3.3. Basement depth estimation

3.3.1. Two–dimensional gravity modelling

The quantitative interpretation of the Bouguer gravity anomaly map is applied through Oasis Montaj Programs (2008). The 2D magnetic modelling technique was applied along five long extended gravity anomaly profiles passing through the major gravity anomalies in the study area. The selected profiles were taken from BAM denoted as P1, P2, P3, P4, and P5 as shown in (Figure 5). All profiles are taken with direction from west to east. The five models are shown in (Figure 5), where the 2D gravity modelling reveals a depth of basement is ranging from 4 km to 7 km. The available well data in the area (SANHUR-1X & WEST HALIF-1) confirms the models.

3.3.2. Three-dimensional gravity modelling

In the present work, the (GYMSYS-3D on Geosoft Oasis Montaj 2008) has been used to calculate the three-dimensional gravity modelling along the study area. The GMSYS 3D programme applies an iterative process; to get the best fit model (Figure 6). The thickness of the sedimentary basin is estimated, depending on a constant density contrast between the sediments (2.1 gm/cm3) and the basement (2.67 gm/cm3) (Araffa et al. 2015). The Final 3D gravity modelling results include two main parts, topographic surface and basement rocks as shown in Figure (Figure 6). The 3D model shows that the depth to basement ranges from about 4100 m to ~7000 m, which is compatible with 2D gravity modelling and the available well data

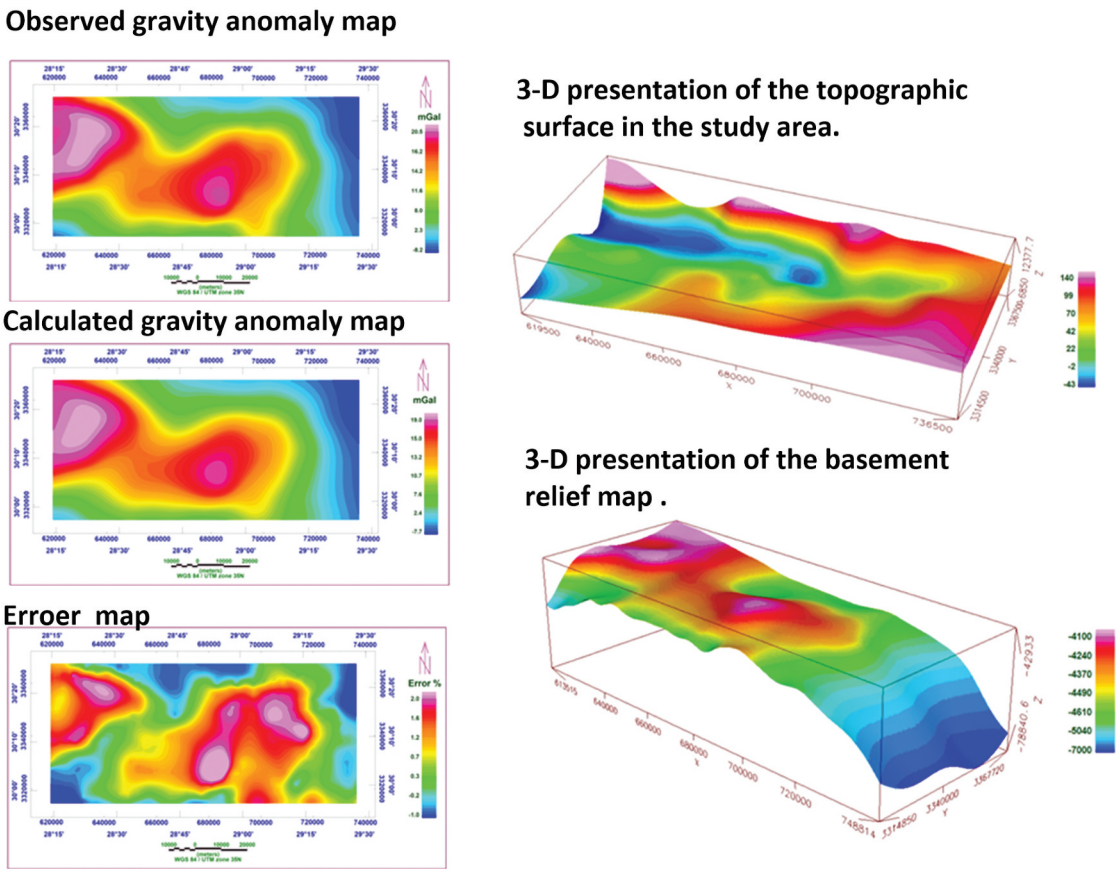

Figure 6. 3D Gravity modelling.

(SANHUR-1X & WEST HALIF-1) in the area (Figure 5). The total depth of SANHUR-1X is (TD = 2832 m) and just reaches the lower Cretaceous and the total depth of WEST HALIF-1 is (TD = 3084 m) and reaches only Kharita formation (EGPC 1992). The depths to the basement at the eastern and southwestern parts of the study are more than 7000 m which indicates that a thick sedimentary cover (basin), whereas depths decrease gradually in central and northwestern directions to reach less than 4100 m. Such structures are controlled by faults, as confirmed by Euler and TDR filters.

4. Discussion

Results of gravity data delineate the structural fault elements that are deduced from different filters such as: high pass filter, Euler deconvolution, and tilt derivative filter, which exhibit main trends such as E–W, ENE–WSW, and N–S. The depth to basement rocks deduced from 2D gravity modelling is compatible with the results of 3D gravity modelling, which ranges from ~4000 to ~7000 m. Also, the depths calculated by Euler deconvolution are more than 4000 m. Salem et al. (2012) calculated the depth to the basement at the area located south of the study area and concluded that the basement depth ranging from 1.5 to 7 km. Also, the two boreholes UMBARAKA and KATTANIYA-1, drilled outside the study area, reached the top of the basement surface at depths of 4132 m and 4158 m respectively (EGPC 1992), which is near our shallower estimates to the top of the basement.

5. Conclusion

Results of gravity data interpretation indicate that the most tectonic trends are generally aligned in E–W, ENE–WSW, and N-S for the major structures, while the minor structures are aligned in the directions NNE–SSW, NE–SW, NNW–SSE, and NW–SE. The depth of crystalline basement rocks are ranging from ~4100 m to ~7000 m. Basement are deeper (7000 m) at the eastern and southwestern parts of the study area, which indicate a thick sedimentary cover (basin), but they decrease gradually in central and northwestern directions to reach depths of less than 4100 m. The great thickness of sedimentary cover in the eastern part could be possible hydrocarbon accumulation in the main basin or sub-basins.

Disclosure statement

No potential conflict of interest was reported by the author(s).

ORCID

Sultan A.S. A. S. Araffa http://orcid.org/0000-0002-7098-918X

References

Abd El-Azeem M, El-Sawy KE, Gobashy MM. 2013. Analysis of magnetic gradients at North East of Wadi Ar Rika quadrangle, Saudi Arabia, to delineate subsurface linear features and faults. NRIAG J Astron Geophys. 2 (1):27–38. doi:10.1016/j.nrjag.2013.06.006.

Abdelazeem M, Fathy MS, Gobashy MM. 2021. Magnetometric identification of sub-basins for hydrocarbon potentialities in qattara ridge. north Western desert (Egypt). PAAG, accepted.

Abdelazeem M, Salem ZE, Fathy MS. 2020. Impact of lithofacies and structures on the hydrogeochemistry of the lower Miocene aquifer at Moghra Oasis, North Western Desert, Egypt. Nat Resour Res. 29(6):3789–3817. December 2020. doi:10.1007/s11053-020-09679-3.

Araffa SAS, El Shayeb HM, Abu-Hashish MF, Hassan NM. 2015. Delineating subsurface structures and assessment of groundwater aquifer using integrated geophysical interpretation at the central part of Sinai, Egypt. Arabian J Geosci. 8(10):7993–8007. doi:10.1007/s12517-015-1824-5.

Araffa SAS, Santos FM, Arafa-Hamed T. 2014. Assessment of subsurface structural elements around greater Cairo by using integrated geophysical tools, Environ. Earth Sci. 71(8):3293–3305. doi:10.1007/s12665-013-2716-1.

Azeem MA, Mekkawi M, Gobashy M. 2014. Subsurface structures using a new integrated geophysical analysis, South Aswan, Egypt. Arab J Geosci. 7(12):5141–5157. doi:10.1007/s12517-013-1140-x.

Blakely RJ. 1995. Potential theory in gravity and magnetic applications. Cambridge (UK): Cambridge University Press.

CONOCO. 1987. Geological map of Egypt, scale 1:500,000.

EGPC. 1992. Western Desert oil and gas fields, The Egyptian general petroleum corporation. p. 428.

Essa W, 2015. Analysis and interpretation of airborne magnetic and gamma-ray spectrometric survey data of gabel umm tineidba area, South Eastern Desert, Egypt. M.Sc. Thesis Fac. Sci. Helwan Univ. 206.

Fergany E, Mekkawi M, Abdel Azeem M, Khalil A. 2014. Integrated geologic and geophysical studies of north unstable shelf seismicity, Egypt. Arab J Geosci. doi:10.1007/s12517-014-1620-7

General Petroleum Company. 1984. Gravity map of Egypt with scale 1:250,000. Egyptian academy of scientific research and technology. Cairo.

Jacobsen BH. 1987. A case for upward continuation as standard separation filter for potential-field maps. Geophysics. 52(8):1138–1148. doi:10.1190/1.1442378.

Oasis Montaj Programs. 2008. Geosoft mapping and processing system: version 7.0.1 (HJ), Inc Suit 500. Richmound St. West Toronto (ON Canada N5SIV6).

Omara S, Sanad S. 1975. Rock stratigraphy and structural feature of the area between Wadi El Natrun and the Moghra depression (Western Desert), Egypt. Geol Jahrb. 16:45–73.

Pickford M, Miller ER, El-Barkooky AN. 2009. Suidae and Sanitheriidae from Wadi Moghra, Early Miocene, Egypt. Acta Palaeontol Polonica. 55(1):1–11. doi:10.4202/app.2009.0015.

Said R. 1962. The geology of Egypt. Amsterdam (New York): El-Sevier Publ. Co; p. 377.

Salem AA, Green C, Fairhead D, Aboud E. 2012. Mapping basement relief of Abu Gharadig Basin, Western Desert of Egypt using 3D inversion of pseudo-gravity data. ASEG Extended Abstr. 2012(1):1–4. doi:10.1071/ASEG2012ab385.

Shalaby MR, Hakimi MH, Abdullah WH, Islam MDA. 2016. Implications of controllingn factors in evolving reservoir quality of the Khatatba Formation, Western Desert, Egypt. Sci Bruneiana Spec Issue Geol. 15. doi:10.46537/scibru.v15i0.39.

Sultan SA, Mekhemer HM, Santos FM. 2009. Groundwater exploration and evaluation by using geophysical interpretation (case study: al Qantara East.. Arabian Geosci J Springer. 2(3):199–211. doi:10.1007/s12517-008-0028-7.

Telford WL, Sheriff R, . 1990. Applied geophysics. Second. Cambridge Univ. Press; p. 660.